Supplementary Information:

Triboelectricity-Driven Chemistry at Oppositely Charged Triboelectric Interfaces with Ionic Dyes

Experimental Procedures

Materials:

Cupper electrode, Polytetrafluoroethylene (PTFE), Polyamide 6,6 (PA-66), Methyl orange (MO) – an anionic dye, Basic blue 40 or Cationic blue (CB) – a cationic dye.

Chemical Reagents:

P-benzoquinone ($C_6H_4O_2$, 99.5%) was purchased from Shanghai Macklin Biochemical Technology Co., Ltd.

Tert-butanol (98.0%) was purchased from Sinopharm Chemical Reagent Co., Ltd.

Sample Preparation:

2 cm^2 films of PTFE and PA were cut to perform the solid-solid and solid-liquid TENG measurement.

A 5-ppm aqueous MO and CB solution was prepared by adding 5 mg of $C_{14}H_{14}N_3NaO_3S$ and $C_{37}H_{34}N_2Na_2O_9S_3$ to 1 liter of deionized water, followed by magnetic stirring for 1 h.

Each ultrasonication sample consisted of 20 mL of a 5 ppm MO or CB solution with 30 balls (4 mm diameter) of PTFE or PA. For the combined PTFE–PA samples, 15 balls of each material were used. Aliquots (1 mL) were collected at 0, 1, 2, 3, and 4 hours during ultrasonication for subsequent UV–Vis analysis. The ultrasonic bath temperature was maintained at 20 °C, with a frequency of 40 kHz and a power of 500 W. When an ultrasound power of 120 W was used, it is explicitly stated; otherwise, the default operating power was 500 W.

Each sample for ball milling contained a PTFE vial and 50ml of 5ppm MO or CB solutions with 1200 balls of either PTFE or PA of 4mm diameter. 1ml aliquots were sampled at 0, 1, 2, 3, and 4-hour intervals during ball grinding for the subsequent UV-Vis measurements. The milling speed was set at 360 RPM for each run, with a seven-minute run and three-minute rest to minimize the heating effect.

Sample Characterization:

Water's static contact angles were determined using a DSA-100 optical CA meter (Kruss Company, Ltd., Germany) with a test temperature set at room temperature.

TENG measurement were performed via linear motor LinMotS01-72/500

The UV-Vis absorption spectra of samples were recorded with a Hitachi UV-4150 UV-Visible spectrometer on a range of 200 -700 nm.

Methods:

The droplets were dispensed using an automatic digital pipette gun (Brand: OEM) equipped with a plastic pipette needle (inner volume of pipette: 1-200 μl). The pipette was positioned at a fixed height of 1 mm above the triboelectric surface. Each droplet was released by gun guided by gravity upon achieving a volume-defined on scale, ensuring consistent initial contact conditions. Droplet impact and spreading behavior were monitored using a high-speed camera (Model iPhone 17 Pro Max, Brand) operating at 240 fps at 1080p. This allowed us to confirm that the contact area and separation dynamics were consistent across repeated trials for each droplet volume. Any trials exhibiting splashing, satellite droplet formation, or asymmetric wetting were excluded from analysis. For each droplet volume condition (e.g., 0, 50, 100, 150, 200 μl), a minimum of 3–7 repeated contact separation cycles were performed and analyzed. The output values presented in Figure 2 represent the mean ± standard deviation calculated from these replicate measurements.

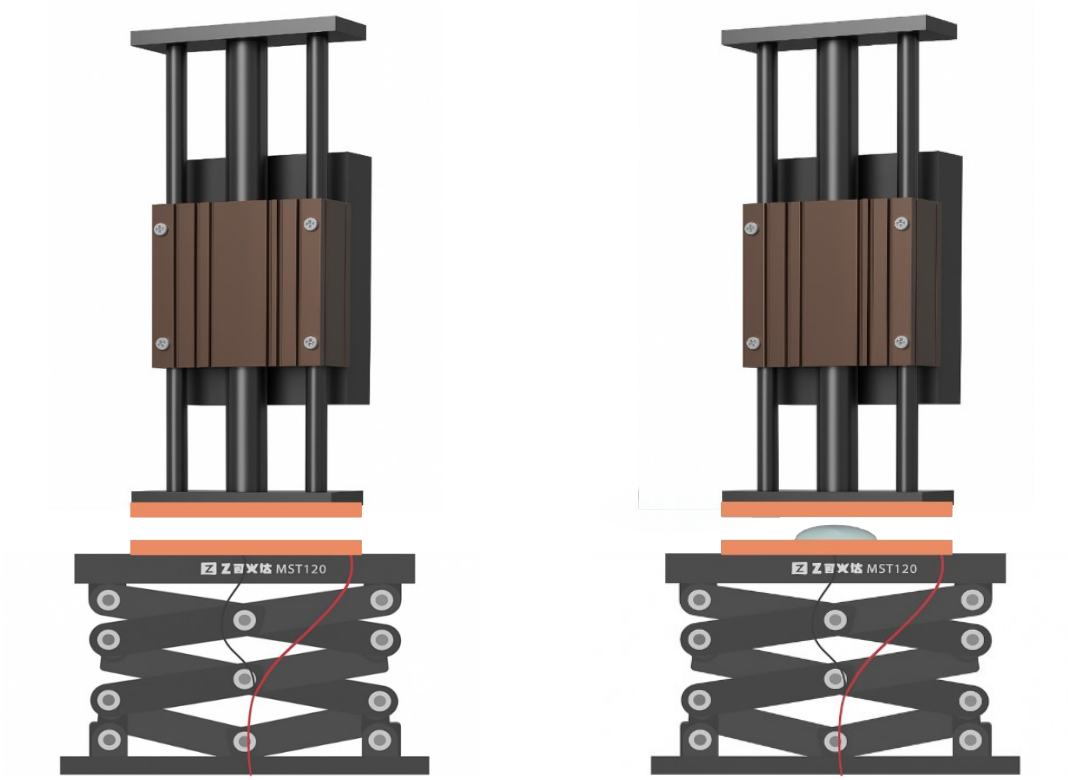

Figure S1: Illustration of the experimental setup of a Solid-Solid and Solid-Liquid TENG

(a) **(b)**

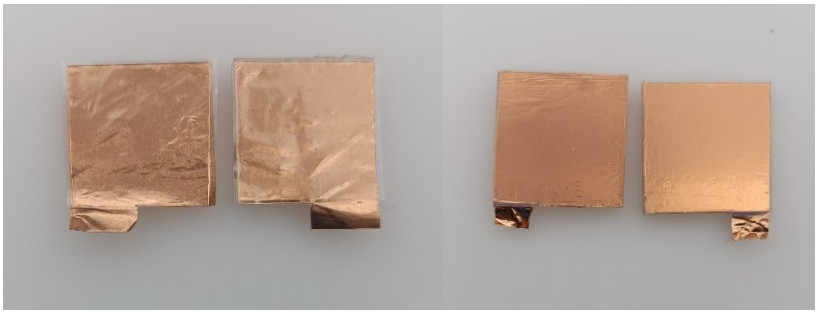

Figure S2: Photographs of copper electrode with 2.5cm^2 dielectric material sheets present on it (a) PA (b) PTFE

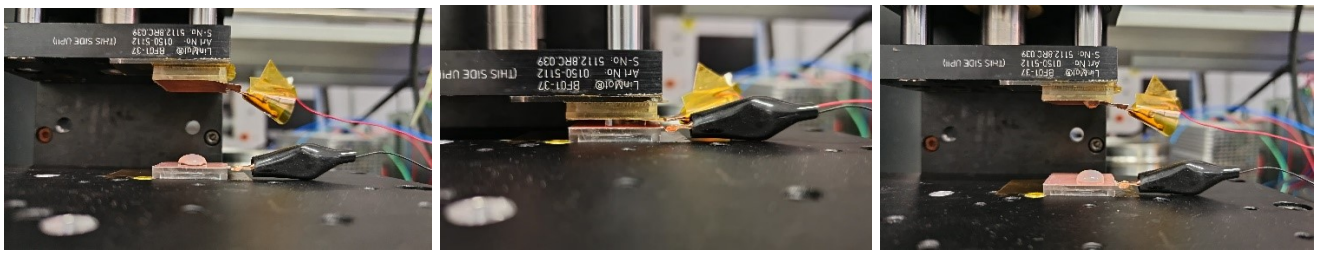

Figure S3: PA-PTFE SL-TENG photograph of one cycle squeezing a 250µl water droplet. Water is attracted to the hydrophilic PA surface, which is mounted on top.

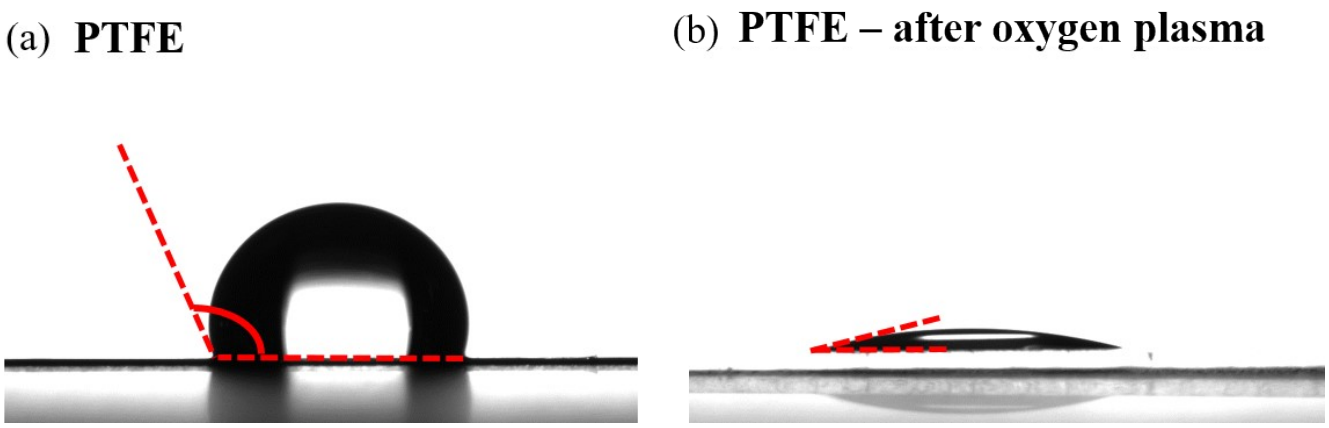

Figure S4: Contact angle measurement of water and PTFE (a) before and (b) after the oxygen plasma treatment.

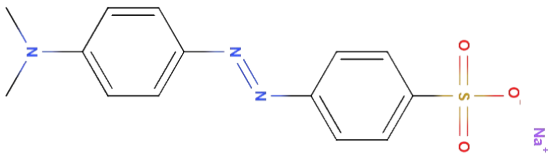

Figure S5: Molecular Structure of MO

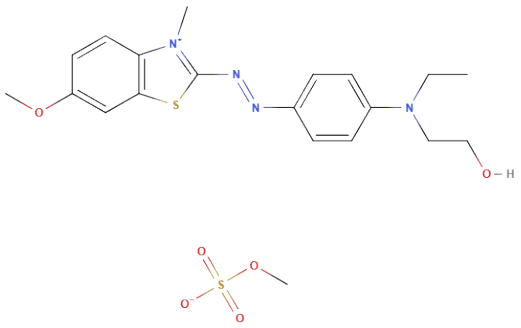

Figure S6: Molecular Structure of CB

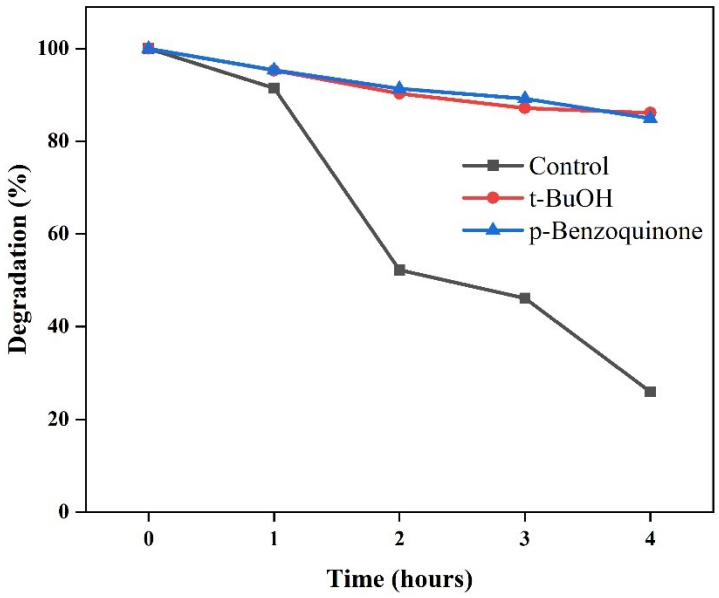

Figure S7: Evolution of relative concentration of CB under various radical scavengers with the same final concentration of 1mM. The relative concentration is calculated based on the absorbance of CB, that measured by UV-Vis spectroscopy.

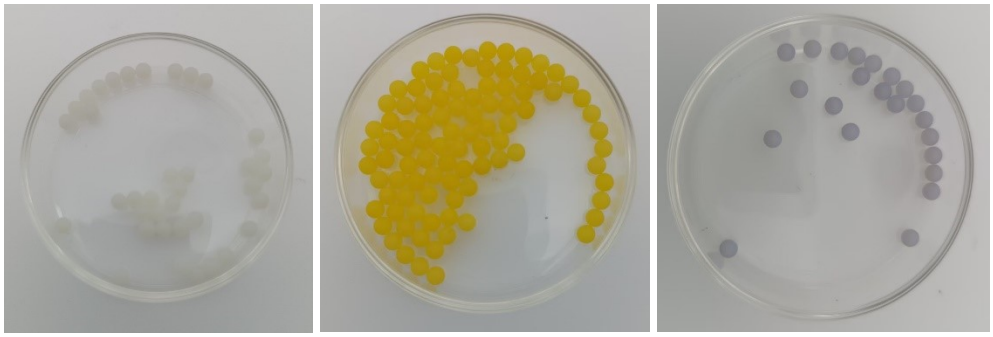

Figure S8: Photographs of PA balls (a) before ultrasonication. After four hours of ultrasonication with (b) MO (c) CB

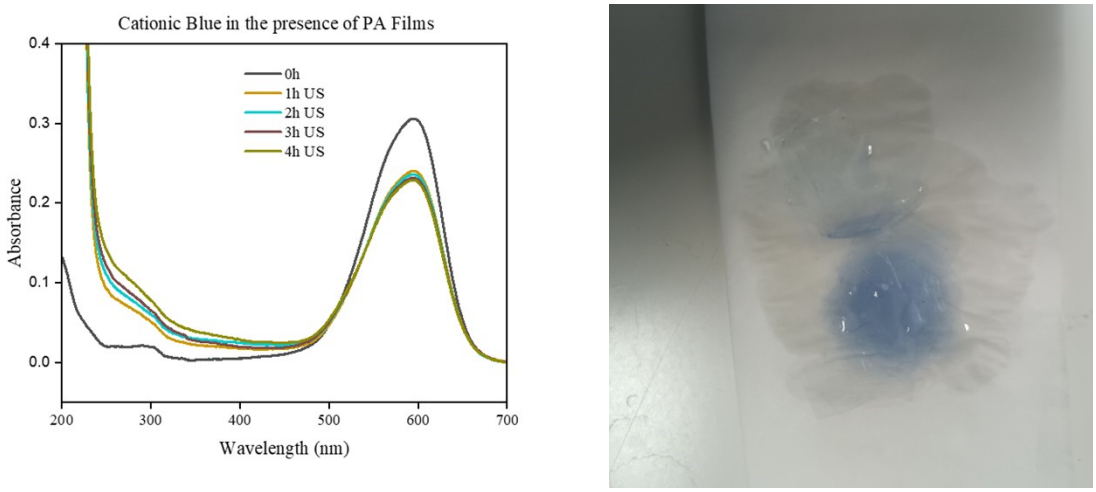

Figure S9: (a) Inhibition of CB degradation in the presence of PA films. (b) Photograph of PA films after 4h ultrasonication.

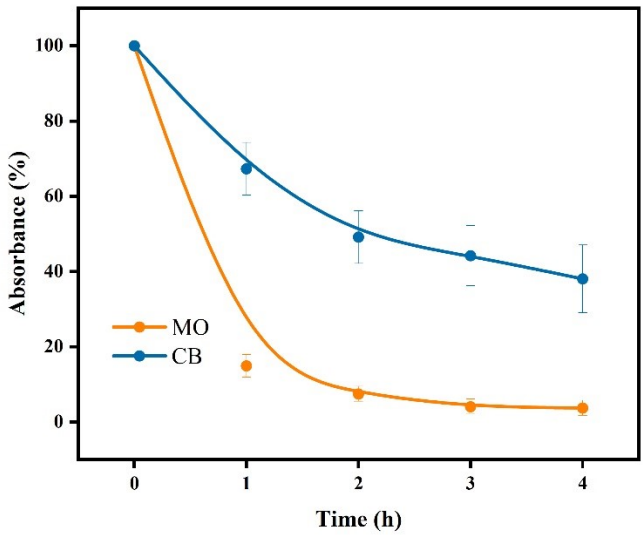

Figure S10: Relative concentration of MO and CB in the presence of 15 PTFE and 15 PA balls for four hours.

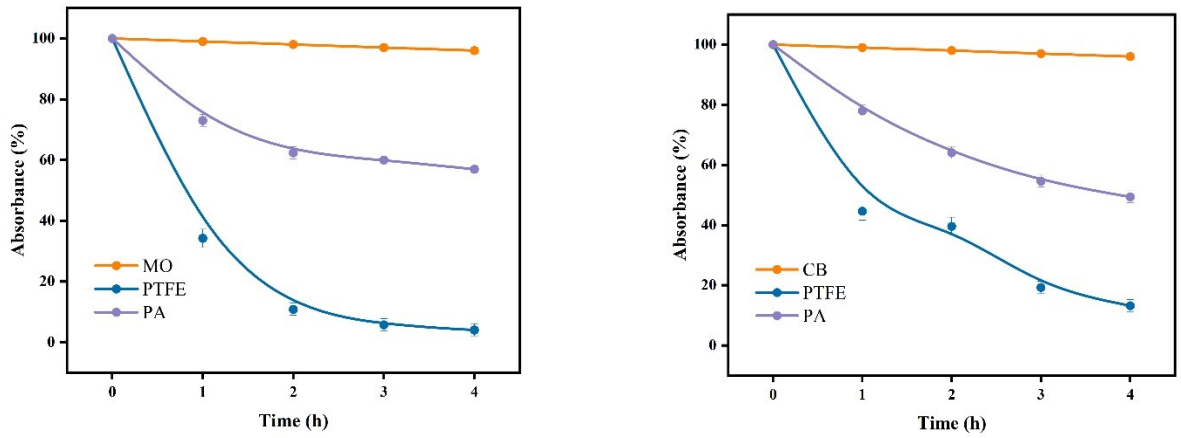

Figure S11: Absorbance evolution of (a) MO and (b) CB in the presence of different dielectric materials. Ultrasound parameters: 40kHz and 120W.

Time	Degradation
0 hour	0%
1 hour	65%
2 hour	84%
3 hour	95%
4 hour	99%

Time	Degradation
0 hour	0%
1 hour	55%
2 hour	60%
3 hour	80%
4 hour	86%

Table S1: Degradation percentage of 20ml (a) MO and (b) CB in the presence of 30 PTFE balls via ultrasound-induced CEC. Ultrasound parameters: 40kHz and 120W.

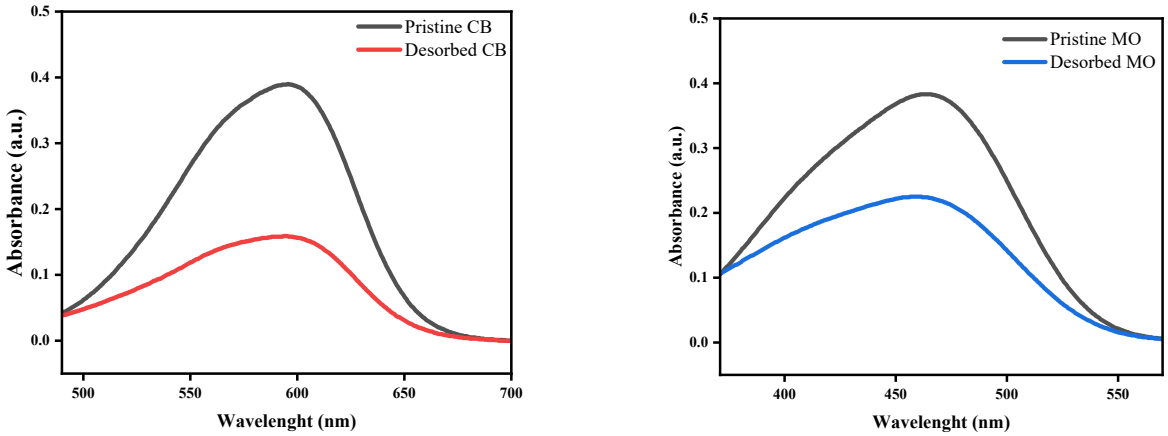

Figure S12: Desorption spectrum of (a) CB (b) MO

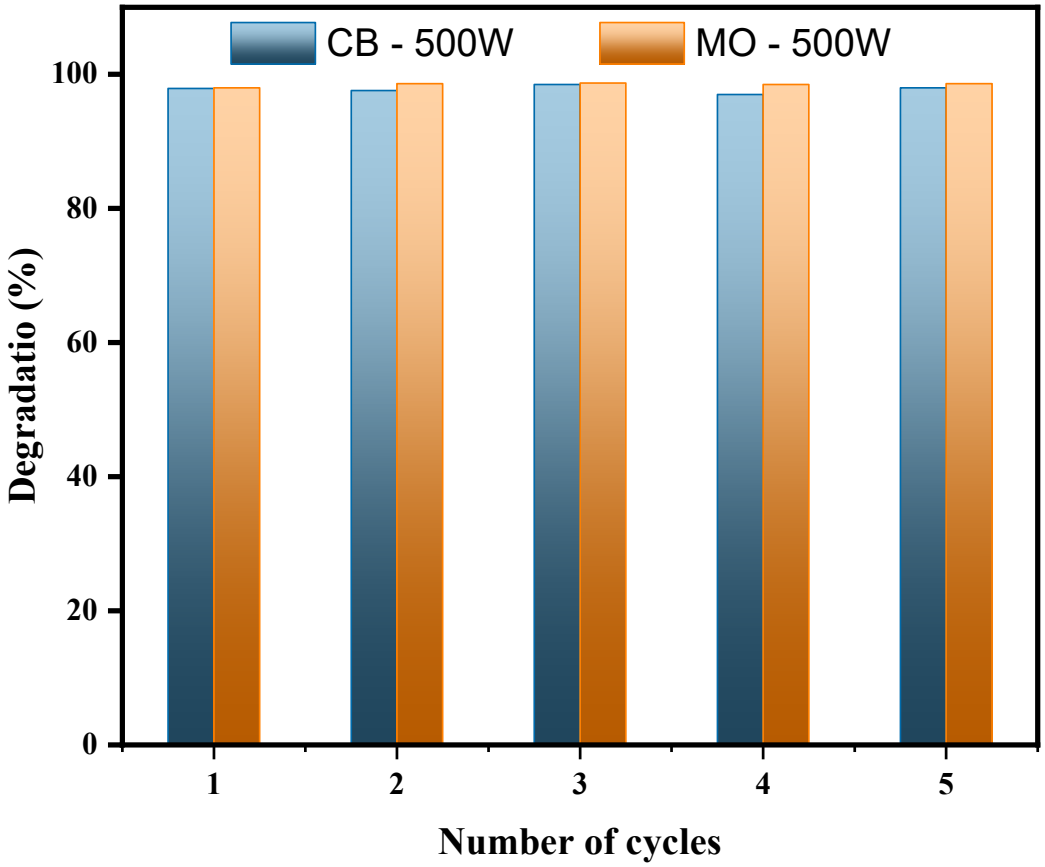

Figure S13: Repeated performance of PTFE balls for five cycles of 1h each.

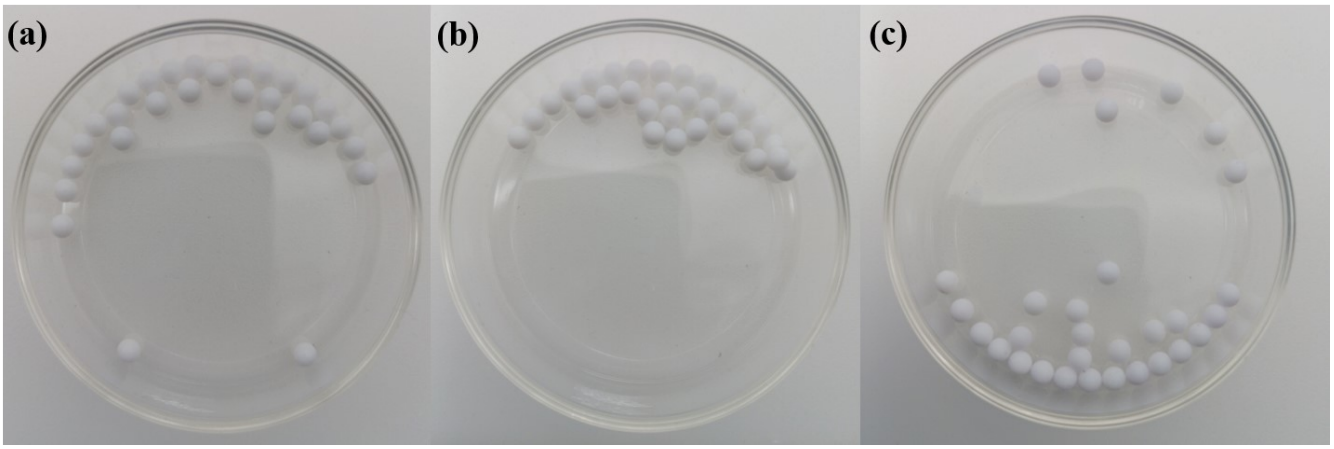

Figure S14: (a) PTFE balls before CE-Chemistry (b) after 5 repeated cycles of ultrasonication with MO (c) after 5 repeated cycles of ultrasonication with CB

Dielectric Materials	Young's modulus (GPa)
PTFE	0.5 – 1.0 (very soft & compliant)
PA	2.0 – 3.5 (moderately stiff & tough)

Table S2: Typical Young's modulus values of dielectric materials

Dielectric Materials	Mass (g)
PTFE	87.36g
PA	45g

Table S3: Mass of 1200 dielectric balls of 4mm diameter

Out[•]=

rd (m)	0.141
rv (m)	0.04
ωd (rad/s)	$\frac{10\pi}{3}$
ωv (rad/s)	$-\frac{20\pi}{3}$
phi1 (rad)	1.4142136×10^{-6}
T1 (s)	6.7523724×10^{-8}
T2 (s)	0.01
T3 (s)	0.31
Cycle T (s)	0.32
Frequency f (Hz)	3.125
Detaching speed |v1| (m/s)	0.219911

Table S4: The following parameters are set in Wolfram Mathematica to calculate and compute the frequency, power and kinetic energy of collisions between the vials and the balls.

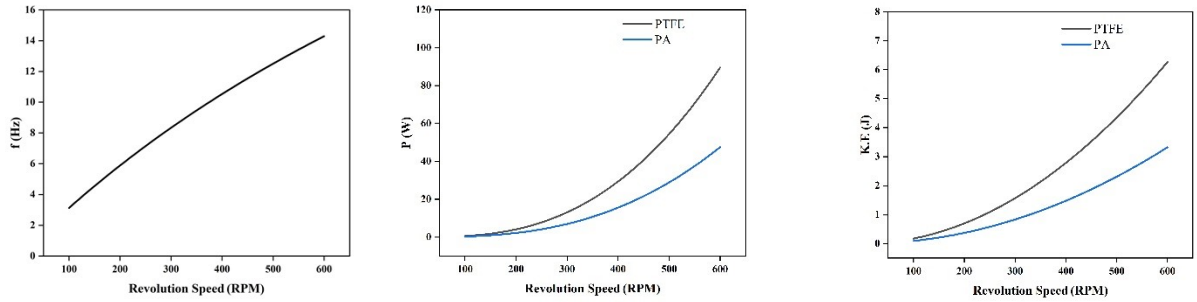

Figure S15: The above calculations are performed via theoretical methods presented in the supplementary note 2 of the reference.[1] A code was written using equations 1-18 and manually run via Wolfram Mathematica. The parameters are shown in the table S2.

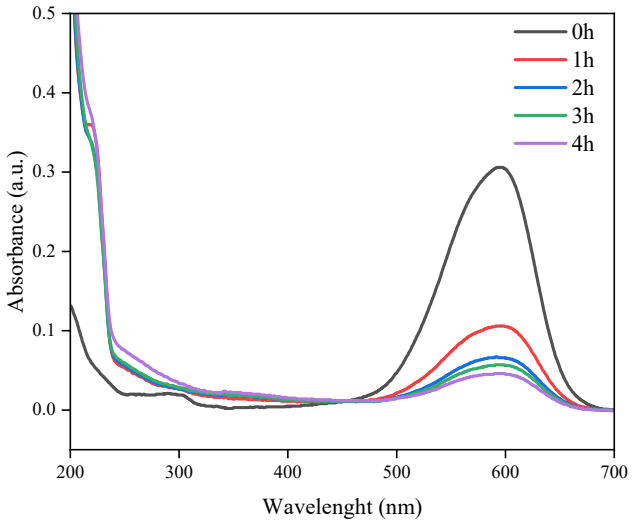

Figure S16: The UV-vis spectra of the CB solution in the presence of 1200 PTFE balls via ball milling.

Figure S17: (a) Shows the ball milling vial after 4h of operation with balls 50ml solution of CB (b) shows the balls with adsorbed CB on the surfaces after 4h of milling. (c) shows the PTFE milling vial with adsorbed CB after 4h of milling.

Time	Degradation
0 hour	0%
1 hour	70%
2 hour	80%
3 hour	99%
4 hour	99%

Time	Degradation
0 hour	0%
1 hour	65%
2 hour	78%
3 hour	81%
4 hour	84%

Table S5: Degradation percentage of 50ml (a) MO and (b) CB in the presence of 1200 PTFE balls via ball milling.

Figure S18: (a) photograph of 1200 PA balls with 50ml solution of MO in the PTFE vial after 4 hours of milling. (b) Adsorbed MO on the PA balls after 4 hours of continuous milling.

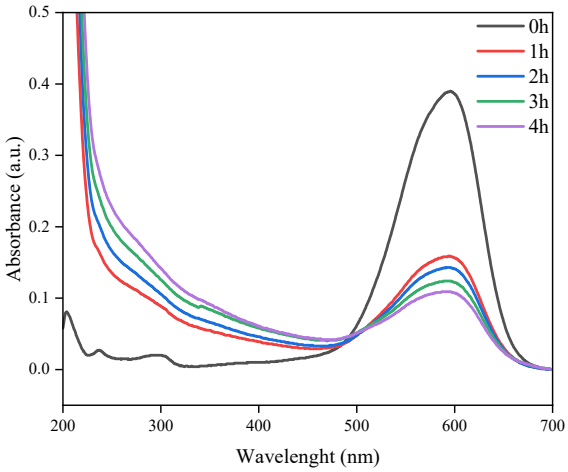

Figure S19: The UV-vis spectra of the CB solution in the presence of 1200 PA balls via ball milling.

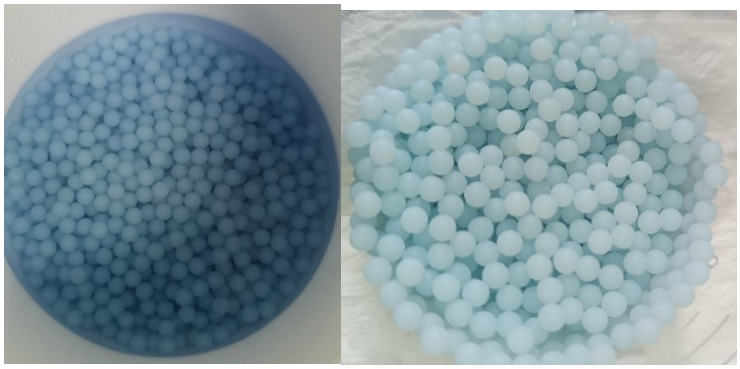

Figure S20: (a) photograph of 1200 PA balls with 50ml solution of CB in the PTFE vial after 4 hours of milling. (b) Adsorbed CB on the PA balls after 4 hours of continuous milling.

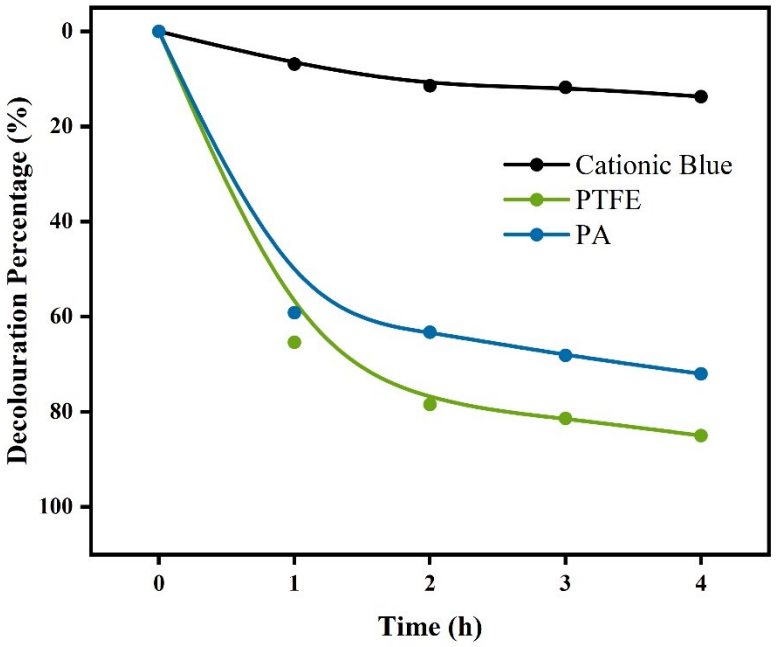

Figure S21: Decrease in relative concentration of CB in the presence of various dielectric materials via ball milling.

PTFE	PA
Degradation via triboelectric charge	Adsorption inhibits the degradation

Table S6: Ball milling experimental results with different triboelectric materials.

Supplementary Note 1: Ultrasound parameters

Ultrasound operating conditions dictate whether physical or chemical effects dominate, with frequency and power being the most critical parameters. At relatively low frequencies (<100 kHz) and low power levels (<200 W), physical effects are predominant, while radical generation and sonolysis remain minimal; such conditions are typically classified as low-frequency ultrasound (LFUS). Under LFUS, cavitation-induced physical phenomena, play a central role in accelerating reaction kinetics. In addition, species (mainly solid particles) located near the collapsing bubble interface experience intense localized shear forces produced by high-velocity microjets, which can activate certain molecules or compounds to undergo mechanochemical responses. This has led to the development of mechano-active catalytic systems that exploit externally applied mechanical energy to promote chemical reactions. Among the most recognized examples are piezocatalysis and contact-electro-catalysis (CEC), both of which rely on the mechanical effects generated by ultrasound to drive reaction pathways. In these systems, the ultrasound frequency is typically maintained at or below 40 kHz, with the applied power kept below 200 W, to ensure the predominance of physical cavitation effects. Under these conditions, the contribution of direct chemical effects of ultrasound, such as radical formation and sonolysis, remains minimal and does not significantly influence or override the intrinsic reaction kinetics.[2]

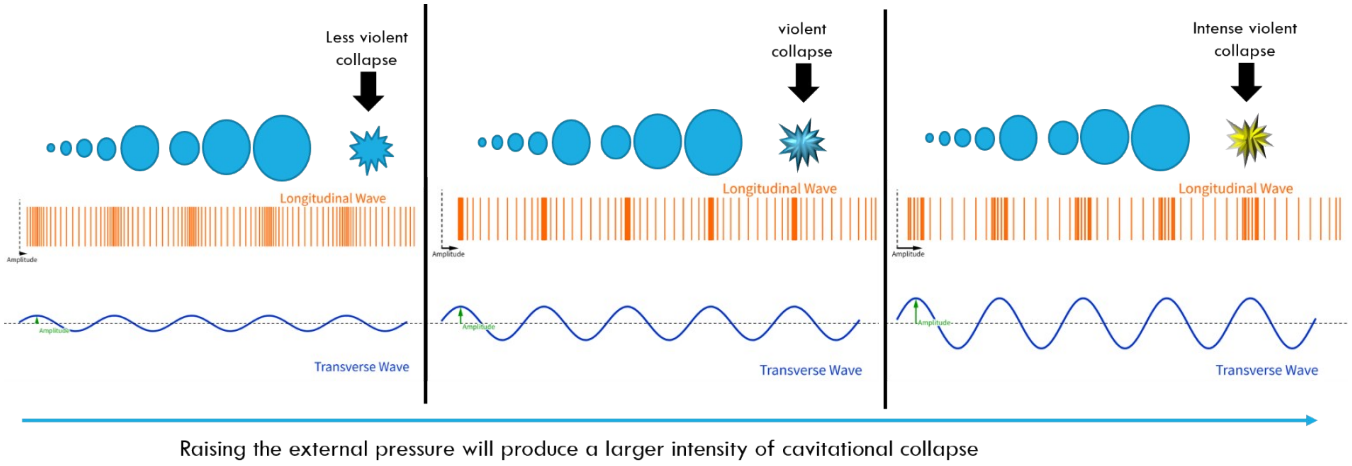

Supplementary Note 1 figure 1: Visual illustration of increasing in cavitational collapse with the increase of ultrasound power created using GeoGebra

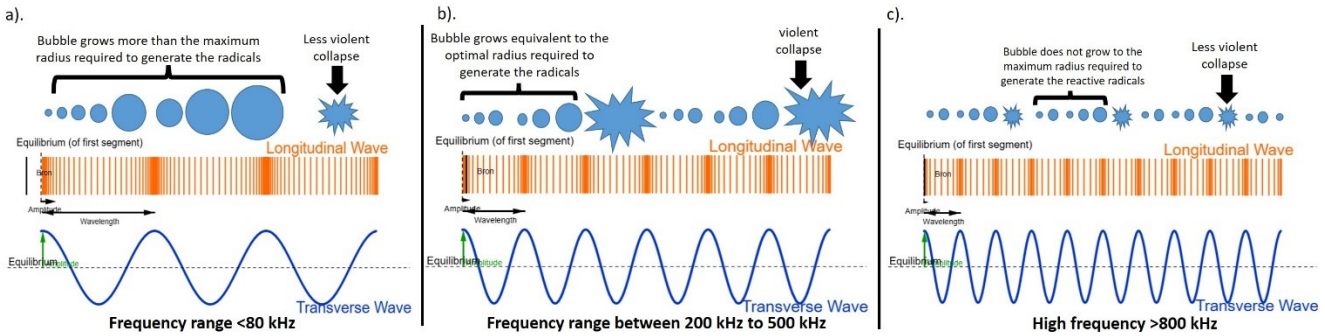

Supplementary Note1 figure 2: Different frequency ranges and their effects at constant power. a) Low-frequency ultrasound; bubbles grow more than the maximum radius for the generation of radicals; therefore, chemical effects are negligible while physical effects dominate. b) Optimal frequency range for radical generation, i.e., bubble size is favorable to the required radius for the radical generation; therefore, chemical effects dominate. c) Bubble radius is less than the required minimum radius for the generation of reactive radicals. Reproduced with the permission of the reference [2], copyright Elsevier 2025.

Supplementary Note 2: Adsorption and EDL regulation

It is proposed that, although adsorption and EDL formation are inherently coupled, distinct roles are played by them at different stages of dielectric solid-liquid contact electrification. In such systems, charge generation is initiated primarily by interfacial electron transfer upon contact, after which ionic migration and redistribution occur to compensate and stabilize the emerging surface charge. Under these conditions, adsorption, defined as the site-specific attachment of ions or charged species driven by chemical affinity, surface functional groups, and local electrostatic interactions, can rapidly occupy the outermost layer of the solid surface, particularly when strongly interacting functional groups are present. This interfacial occupation alters the local electronic environment and, consequently, the effective triboelectric properties, thereby modifying the initial electron-transfer behaviour that governs charge generation. Following this primary charge-transfer event, the EDL is established through the subsequent migration and spatial organization of mobile ions near the charged interface, forming a diffuse screening structure that compensates the surface potential. Thus, while adsorption directly reshapes the surface states that determine the propensity for electron transfer at the earliest stage, the EDL predominantly governs the post-transfer processes, including charge stabilization, screening, recombination dynamics, and the transient displacement currents generated during contact-separation cycles. Within this framework, adsorption acts as a rapid interfacial modifier that can redefine the intrinsic charging characteristics. This stage-resolved perspective clarifies their relative importance and provides a mechanistic basis for understanding how surface chemistry and interfacial ion dynamics jointly control CE-Chemistry kinetics.

Supplementary Note 3: Calculation of percentage efficiency for Ball Milling vs Ultrasound

For each ultrasonication experiment, 30 PTFE balls were employed to treat 20 mL of the dye solution. In contrast, each ball-milling experiment utilized 1200 balls with 50 mL. In both cases 5-ppm dye solution for a duration of 4 hours was employed. It is supposed that both mechanochemically driven processes achieved 100% degradation within these 4 hours.

Efficiency Calculation

We can now calculate a simple and powerful metric: "Dye Processing Capacity per Ball."

Ultrasound Efficiency:

20 ml / 30 balls = 0.667 ml/ball

Ball Milling Efficiency:

50 ml / 1200 balls = 0.0417 ml/ball

Relative Efficiency (Ultrasound vs. Ball Milling):

(0.667 ml/ball) / (0.0417 ml/ball) = 16

Conclusion and Interpretation

The ultrasound process is 16 times more efficient per ball than the ball milling process under these conditions. This means that, on average, each individual ball in the ultrasound reactor is 16 times more effective at degrading the dye than each individual ball in the ball mill.

Supplemental References:

[1] Z. Wang *et al.*, "A contact-electro-catalysis process for producing reactive oxygen species by ball milling of triboelectric materials," *Nature Communications,* vol. 15, no. 1, p. 757, 2024.

[2] S. T. Muntaha, Z. L. Wang, and D. Wei, "Reevaluating Mechano-driven Chemical Reactions: Insights from Ultrasonic, Piezo, and Contact-Electro Mechanisms," *Electrochimica Acta,* p. 147563, 2025.